Journal of proteome research

Cite This: J. Proteome Res. 2018, 17, 1532−1546

Article

pubs.acs.org/jpr

Quantitative Proteomics and Cytology of Rice Pollen Sterol-Rich Membrane Domains Reveals Pre-established Cell Polarity Cues in Mature Pollen

Bing Han,[†,‡,∥,⊥] Ning Yang,[†,‡,∥] Hai Pu,[§] and Tai Wang*[,‡,∥]

[‡]Key Laboratory of Plant Molecular Physiology, Institute of Botany, Chinese Academy of Sciences, Beijing 100093, China

[§]Bruker Daltonics Inc. (China), Beijing 100081, China

[∥]University of Chinese Academy of Sciences, Beijing 100049, China

Supporting Information

ABSTRACT: Cell polarity is essential for generating diverse cell functions. The underlying mechanisms of how a cell establishes, maintains, and changes its polarity are poorly understood. Recently, sterol-rich membrane microdomains are found to be associated with these processes. However, both its exact characteristics and importance are still unclear. Here we show microdomains change dynamically in developing and germinating rice pollen with selective enrichment in the aperture and the tip of newly born pollen tubes by use of the sterol-specific probe filipin. Using the sterol extraction sensitivities of microdomain proteins and quantitative proteomics, we identified 237 microdomain-associated proteins from 934 identified pollen detergent resistant membrane proteins. This proteome includes almost all of the known key regulators comprising the polar growth network, and it shows more similarity to front−back polarized HeLa cells than nonpolarized *Arabidopsis* suspension cells. We immunolocalize flotilin-like protein, a representative of these sterol-dependent proteins and directly visualize microdomains in pollen. These results indicate the presence of microdomains in pollen and pre-established cell polarity around the aperture during pollen maturation. Our findings reveal an atlas of the microdomain-associated proteome in pollen. This work provides useful resources and knowledge needed to further dissect the mechanisms for the establishment and maintenance of cell polarity.

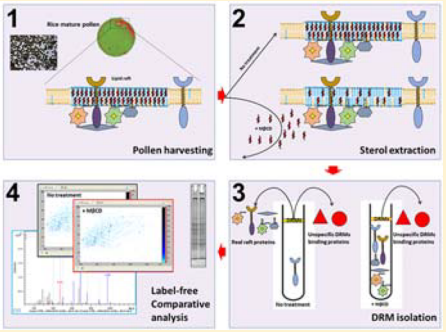

KEYWORDS: *cell asymmetry, filipin, sterol-rich membrane microdomains, label-free quantitative proteomics, methyl-β-cyclodextrin (MβCD), polar growth, pollen tube, rice pollen*

INTRODUCTION

In contrast to animals, where sperm is directly generated through the process of meiosis, flowering plants generate sperm cells via a specific postmeiotic process.[1] During this process, meiosis of pollen mother cells generates microspores that undergo asymmetric mitosis to yield a large vegetative cell and a smaller generative cell that is enclosed within the vegetative cell.[1,2] The vegetative cell is terminally differentiated, whereas the generative cell further divides to produce two sperm cells. After pollination, the vegetative cell hydrates on the stigma and bulges from germination aperture.[3] Eventually, this bulge extends directionally to form a tip-growing pollen tube for delivering the two sperm cells into the embryo sac for double fertilization.[4]

Cell polarity involves the asymmetric distribution of cellular determinants along a particular axis within a cell and is essential for generating diverse cell functions such as cellular communication, cell division, cell morphogenesis, and differentiation. Thus, polarity is linked to the development and functionality of an entire organism.[5,6] It is very critical but still unclear how a cell establishes, maintains, and changes its polarity in response to intracellular and extracellular stimuli.[7] The pollen tube is one of the excellent model systems to address these questions. Studies have revealed a set of signal molecules essential for tip growth of the tube such as Rho-related small GTPases from plants (ROPs), receptor-like kinases (RLKs) and phospholipids, and the central role of ROPs in the tip growth.[8] The function of these signal molecules depends on their apical plasma membrane (PM) localization. Loss of the apical PM localization leads to severe depolarization of the tube.[9] How these signal molecules are targeted to and maintained in the apical domain is largely unknown, although several studies showed that the ROP negative regulators RopGAP and RopGDI were implicated in defining ROP activity in the apical domain.[9,10] Evidence also suggests specific endocytosis may be important to maintain signal molecules in the apical domain.[11,12] Furthermore, because pollen tube tip growth is initiated preferentially at the aperture of mature pollen under appropriate conditions, answering whether cell polarity is present and how it is established in mature pollen is crucial for understanding the mechanisms underlying establishment and maintenance of cell polarity.

Received: November 27, 2017
Published: March 6, 2018

DOI: 10.1021/acs.jproteome.7b00852
J. Proteome Res. 2018, 17, 1532−1546

Sterols are essential components of the PM, where sterol-mediated liquid-ordered phase separation drives the formation of sterol-rich membrane microdomains (or lipid rafts). These lateral subcompartments are assumed to be important for spatially organizing specific membrane-associated components to different compartments in a cell, which establishes a diverse milieu of signaling epicenters via lipid−protein and protein−protein interactions.[13,14] When these nanoscale liquid-ordered membrane islets coalesce in certain cell types/under certain cell conditions, a macroscopic cellular asymmetry is generated and the clustered microdomains can be more easily observed. In certain mammalian cells, microdomains display an asymmetrical distribution and could be involved in diverse important biological events including endo- and exocytosis, signaling, cell polarity, an axon and synapse formation and function.[15−18] The asymmetrical distribution of microdomains has also been documented in fungus, yeast, and plant cells.[19−24] In plants, microdomains are in the apical dome of pollen tubes and root hairs. Furthermore, apical sterol complexation caused by filipin, a sterol specific fluorescent probe, arrested tip growth of pollen tubes and root hairs.[23,24] The local enrichment of sterol in a membrane is a useful marker for predicting root hair polarity and the outgrowth site during the prebulge stage,[23] and it is also essential for the polarized localization of auxin transporters PIN1, 2, and 3.[25] The association of *Arabidopsis* AtROP6 with microdomains is regulated by S-acylation and required for AtROP6 signaling during polar growth and apical endocytosis in root hairs.[26] All lines of evidence indicate that microdomains may be key players important for upstream cell polarity cues. However, limitations in the observation of these nanoscale membrane structures make it difficult to carry out studies into microdomain-related processes, especially for cell wall-protected plant and fungal cells.[27] Thus, the molecular features and functions of microdomains in cell polarity are still poorly understood.

High throughput proteomics approaches provide opportunities to identify protein components of microdomains and to establish the framework for understanding their functional relevance with cell polarity. Unlike the organelles and vesicles which have an independent structure and clear-cut boundary, microdomains are less defined lateral subcompartments in the membrane; therefore, there are still not simple and direct methods to biochemically isolate and purify microdomains for proteomic and other biochemical studies currently. Because of the difference in biophysical characteristics of the liquid-ordered microdomains and other membrane areas, the microdomains have differential detergent solubility than other membrane areas. Detergent resistant membranes (DRMs) isolated by cold detergent treatment are widely used in microdomain research.[16,28] However, the correlation between microdomains and DRMs was questioned for lack of direct *in vivo* proofs such as immunolocalization-based visualization.[27,29] It is generally considered that localization of proteins in microdomains is dependent on sterol; disruption of sterol in membrane by use of the sterol chelator methyl-β-cyclodextrin (MβCD) will dissociate microdomain-associated proteins from the microdomains. Actually, the sterol depletion strategy has long been widely used in the studies of caveolae, a well-known subtype of microdomains in animal cells.[30] MβCD-based quantitative proteomics allows discrimination between proteins copurifying in DRM fraction and true proteins dependent on sterol-rich membrane regions.[31,32]

Pollen is the male gametophyte of phanerogamae. It usually consists of one haploid vegetative cell and one or two sperm cells enclosed in the vegetative cell. Mature pollen grains (MPGs) from most phanerogamae species are metabolically quiescent. However, once pollinated onto stigma, the MPG can quickly hydrate and germinate to give rise to a vegetative cell-derived polarized cell structure named a pollen tube (PT) which can arrive at the ovule by oriented growth and deliver the sperm cells into the ovule for double fertilization. The polar growth of the PT is necessary for sexual reproduction of phanerogamae; in addition, it is a typical asymmetrical process of a cell. Therefore, MPGs and pollen tubes are widely used as models in cell asymmetry and polarity research.[24,33] Here, we revealed the dynamic characteristics of sterol-rich membrane microdomains in developing rice pollen using the steriol-specific probe filipin, and we showed selective enrichment around the aperture of pollen. We identified 237 microdomain-associated proteins using a label-free quantitative proteomic comparison of sterol-extracted and control rice pollen DRMs. We visualized microdomains in pollen by use of immunolocalization. The rice pollen microdomain-associated proteome includes most of the known key players of cell polar growth, such as ROPs, ROP-GTPase-activating proteins (ROP-GAP), phosphatidylinositol-4-phosphate 5-kinase (PIP5K), phosphatidylinositol-4,5-bisphosphate 3-kinase (PI3K), calcium ATPase (Ca^{2+} ATPase), pectin methylesterases (PMEs), pectin methylesterases inhibitor (PMEI), and exocyst complex proteins. This polar growth adapted pollen microdomain proteome is more similar to that of HeLa cells than that of *Arabidopsis* suspension cells; even so, rice pollen is very much evolutionarily different from HeLa cell. Considering the HeLa cell is still a front−back polar cell after the epithelial-mesenchymal transition (EMT)[34] while *Arabidopsis* suspension cell is not, this result indicates that the mechanism for cell polarity could share several common features across plant and animal cells.

MATERIALS AND METHODS

Plant materials

Pollen mother cells, dyads, tetrads, microspores, bicellular pollen, and immature tricellular pollen for cytological observation were obtained from rice anthers of different developmental stages by using previously described methods.[35−37]. Mature pollen (MP)[38] and germinated pollen (GP) were obtained from the matured cracked anthers as described previously.[39] The collected MP was dried briefly at room temperature and used immediately or kept at −80 °C until use. All of these materials were obtained from rice cultivar Zhonghua 10 (*Oryza sativa* L. ssp. *japonica*).

Observation of filipin-sterol fluorescence in pollen

Filipin staining was performed as described previously[40] with a few modifications. In brief, fresh samples were fixed in 4% (w/v) paraformaldehyde in a microtubule-stabilizing buffer (50 mM PIPES, 5 mM EGTA, and 5 mM $MgSO_4$, pH 7.0). Filipin III (Sigma) stock solution (10 mg/mL in DMSO) was added to a final concentration of 150 μg/mL, and samples were stained in the dark for 2 h under vacuum. The stained samples were washed three times with the microtubule-stabilizing buffer and observed immediately under fluorescence microscopy (Axio Imager A1, Zeiss). The fluorescence of filipin-sterol complexes was excited with a UV laser coupled with a 387 nm filter and detected with an emission filter of 447 to 531 nm. All images were obtained in parallel by use of identical parameters to compare the intensity of fluorescence signals. The original fluorescence images were then transformed into rainbow pseudocolor through ImageJ software (NIH) for visualizing signal changes.

DOI: 10.1021/acs.jproteome.7b00852
J. Proteome Res. 2018, 17, 1532−1546

Methyl-β-cyclodextrin treatment

MP was treated with a sterol disrupting buffer (60 mM MβCD, 50 mM Tris-HCl pH 7.5, 3 mM EDTA, complete protease inhibitors, Roche Diagnostics) for 1 h at 37 °C as described previously[31] and then eluted 2 times with TECP buffer (50 mM Tris-HCl pH 7.5, 3 mM EDTA, complete protease Inhibitors, Roche Diagnostics).

Preparation and fractionation of detergent resistant membranes

Both sterol-extracted and control MP were homogenized in a homogenization medium (250 mM sucrose, 1 mM $MgCl_2$, 1 mM DTT, 1 mM PMSF, 5 mM NaF, 1 mM $Na_4P_2O_7$, complete protease inhibitors, Roche Diagnostics and 50 mM MOPs/KOH, pH 7.5) with the FastPrep-24 instrument (MP Biomedicals, USA) at 4 °C. After centrifugation at 1,000*g* for 5 min at 4 °C to pellet unbroken cells, large debris, and nuclei, supernatant was centrifuged at 4,800*g* for 5 min at 4 °C to remove mitochondria and plastids and then at 100,000*g* for 1 h at 4 °C to collect total membranes (TMs). The protein concentration of TMs was determined by the Bradford assay[41] with bovine serum albumin used as a standard.

TMs were treated with nonionic detergent Triton X-100 [final concentration 1% (w/v)] for 30 min at 4 °C at a ratio of protein to detergent of 1:1.5 with gentle shaking at 60 rpm. The treated TMs were supplemented with 60% (w/v) OptiPrep to a final concentration of 40% and then overlaid by 30%, 20%, and 0% (w/v) OptiPrep in sequence. Both the detergent and OptiPrep were dissolved in TECP buffer. After gradient centrifugation at 180,000*g* for 4 h at 4 °C (Optima XL-100, SW40 Ti, Beckman Coulter, USA), we fractionated the gradients into 12 fractions from top (1) to bottom (12) for protein and sterol quantification and Western blot analysis. All of the solutions were precooled at 4 °C before use. For mass spectrometry (MS) analysis sampling, the low-density DRM fractions from five independent control and treated replicates were collected, diluted, and pelleted down by ultracentrifugation (please see below for the detailed processing methods).

Quantification of sterol and proteins and Western blotting

Sterol and protein concentration were determined by use of an Amplex Red Kit (Molecular Probes, Eugene, OR, USA) and a Pierce BCA Protein Assay Kit (Thermo Fisher Scientific, Rockford, IL, USA), respectively. For Western blot analysis, proteins were separated on a 12.5% SDS polyacrylamide gel and then electrotransferred onto a polyvinylidenedifluoride membrane with 10 mM 3-cyclohexylamino-1-propanesulfonic acid and 10% (v/v) methanol as previously described.[42] Primary rabbit antibodies used are against rice flotillin-like protein (band_7 protein), eIF-4a (DEAD-box ATP-dependent RNA helicase, Beijing Protein Innovation, Beijing, China) and GAPDH (glyceraldehyde-3-phosphate dehydrogenase, Beijing Protein Innovation, Beijing, China). All were used at 1:1000 dilutions.

Protein separation by 1D SDS-PAGE

The low-density DRM fraction was diluted 5 times with TECP buffer and pelleted by centrifugation at 100,000*g* for 1 h at 4 °C. The pellets were solubilized as described previously[43] with several modifications. Briefly, the pellets were solubilized with a buffer (6 M urea, 2.2 M thiourea, 5 mM EDTA, 0.1% SDS, 2% N-octyl glucoside, and 50 mM Tris-HCl pH 6.8) for 1 h at room temperature with agitation of 30 s every 10 min, sonicated with a probe ultrasonic instrument (VCX105, SONICS, Newtown, CT, USA) for 30 s, and centrifuged at 20,000*g* for 20 min to remove the floating insoluble thin lipids layer. Protein concentration was measured using the Bradford method. To improve SDS-PAGE resolution, proteins were treated with DTT/Iodoacetamide for reduction/alkylization and separated on 1 mm thick 12.5% SDS-PAGE gels. 60 μg of proteins was loaded in each lane. Five above-described replicates of control and treated samples were separated in one gel to reduce errors. The gel was stained with Coomassie Blue to visualize proteins. Then, 10 sample lanes (5 control and 5 treated) were separated longitudinally, and each lane was further horizontally cut into 10 fractions. Each 10 fractions from the same latitude but different lanes formed an independent identification and quantification group (G1 to G10).

In-gel protein digestion

Each gel slice was further cut into 1 mm^3 cubes, destained in a destaining buffer (25 mM NH_4HCO_3 and 50% (V/V) acetonitrile), and then dehydrated with 50% and 100% acetonitrile. After removing the solution, the dehydrated gel cubes were dried with Savant ISS110 SpeedVac Concentrator (Thermo, Marietta, OH, USA). In-gel tryptic digestion was carried out in 25 mM NH_4HCO_3 containing 7.5 ng/μL trypsin at 37 °C for 24 h. All proteins from 100 gel slices were digested in parallel.

Protein identification and label-free quantification

After in-gel digestion, for each analysis group, 10 injections (5 control and 5 treated samples; 8 μL per injection) were conducted for LC-MS data set acquiring and 5 injections (combined the control and treated samples of corresponding group, 15 μL per injection) were conducted for LC-MS/MS. The purpose of conducting LC-MS was to acquire the retention time and intensity information which was used to conduct the statistical analysis and screen the differential peptides. The purpose of LC-MS/MS was to further figure out the proteins belonging to the quantitative peptides.

All LC-MS and LC-MS/MS were performed on a MicrOTOF Q-II Q-TOF mass spectrometer (Bruker Daltonics, Billerica, MA, USA) coupled with a Dionex U3000 nano-LC system (Dionex, Sunnyvale, CA). The LC system operated at a flow rate of 400 nL/min. The mobile phase A was 0.1% formic acid in water, and the phase B was 0.1% formic acid in acetonitrile. A binary gradient from 5% to 40% B in 90 min was used for separation on a homemade 10-cm-long C18 column. All mass spectra were acquired over the range of 50−2,500 *m*/*z*.

For protein identification, 4 precursors were selected for MS2 per scan segment, mass windows for precursor ion selection were changed according to the *m*/*z* value (window 8 Da for *m*/*z* 500−1000, window 10 Da for 1000−1500), the threshold for MS2 triggering was >200, relative collision energy was 25 eV for *m*/*z* 200−500 and 25 eV for *m*/*z* 500−1000, the charge state screening was excluding single charge and 2−5 charge prefer, dynamic exclusion setting was 1 MS/MS or release after 0.25 min. All LC-MS/MS data were processed with DataAnalysis 4.0 SP1 from Bruker Daltonics, and the resulting MGF files were searched using Mascot v2.3 against NCBInr *Oryza sativa* database (410,492 sequences, 20100914) with one missed tryptic cleavage maximum. The peptide mass error was set as ±0.05 Da and the MS/MS mass tolerance as ±0.1 Da. The fixed modification was set as carbamidomethylation (C), and variable modifications as oxidation (M) and deamination (NQ). Decoy database searching is used to remove the random peptides contaminants. The results were filtered with significance

DOI: 10.1021/acs.jproteome.7b00852
J. Proteome Res. 2018, 17, 1532−1546

threshold $p < 0.01$ to make sure that the probability of random matching was less than 0.01%, "Require Bold Red" function was checked, and the ion score cutoff was 10 (any number smaller than 10 will be filtered). All results were also evaluated with false-positive rate below 1% using decoy database search at protein level.

The label-free quantification data were achieved using Proteinscape 2.1 combined with ProfileAnalysis 2.0 (Bruker Daltonics, Billerica, MA, USA). In ProfileAnalysis, a *t* test model was created for peptide quantitation with advanced bucketing settings: the EIC mass window and time window were decided by automatic time alignment function, and the bucket values were normalized using sum of all buckets. Then the results were imported into Proteinscape for protein quantitation. The shared peptides were excluded from the quantitative analysis (Only the unique peptides were used for quantification). Only the peptide results with *t* test model at $p < 0.05$ were used for median algorithm calculation. Peptides which have missing values among biological replicates were also excluded from the quantification.

In silico analysis

Signal peptides, conserved domains, and subcellular localization of proteins were detected by use of SignalP 3.0 (http://www.cbs.dtu.dk/services/SignalP/), the SMART program (http://smart.embl-heidelberg.de/), and TargetP 1.1 (http://www.cbs.dtu.dk/services/TargetP/), respectively. The number and length of transmembrane domains (TMDs) and average of hydrophobicity were predicted by SOSUI (http://harrier.nagahama-i-bio.ac.jp/sosui/sosuiG/sosuigsubmit.html). Posttranslational modifications (glycosylphosphatidylinositol anchor, myristoylation, prenylation, and palmitoylation) were predicted by use of the following tools: big-PI Plant Predictor (http://mendel.imp.ac.at/sat/gpi/plant_server.html) for glycosylphosphatidylinositol (GPI) anchor, PlantsP (http://plantsp.genomics.purdue.edu) for myristoylation, PrePS (http://mendel.imp.ac.at/sat/PrePS/index.html) for prenylation, and CSS-Palm 3.0 local version for palmitoylation. Protein annotations were collected from NCBI (http://www.ncbi.nlm.nih.gov/), UniProt (http://www.uniprot.org/), ARAMEMNON (http://aramemnon.botanik.uni-koeln.de/), RGAP (http://rice.plantbiology.msu.edu/), and TAIR (http://www.arabidopsis.org/).

Antibody development

The anti-flotillin-like protein (BAD23328) polyclonal antiserum was raised in rabbits using the conserved C-terminal domain of the protein as the antigen (Supporting Information Figure S1) (Beijing B&M Biotech CO., LTD).

Immunogold localization of flotillin-like protein in pollen

Fresh materials were immediately fixed in 2% glutaraldehyde and 1.25% paraformaldehyde. Fixed materials were dehydrated step by step with ethanol, embedded in LR white resin (Fluka), and ultrathin-sectioned by Leica ultracut R processor. The sections were blocked with 3% BSA and then incubated with anti-flotillin-like protein (1:100 dilution) or preimmune serum (control, 1:100 dilution) for 2 h at room temperature, followed by washing and incubation with antirabbit IgG-gold (10 nm gold particles, 1:60 dilution, sigma) for 1 h at room temperature. These labeled sections were further rinsed and stained with 2% uranyl acetate for 10 min. Finally, gold particles were observed by transmission electron microscopy (JEOL JEM-1230, Japan).

RESULTS

Filipin-sterol complexes redistribute during pollen development

To examine sterol-rich membrane microdomains, we analyzed sterol patches in rice pollen at different developmental stages with filipin, which can form complexes with sterols and is widely used as a fluorescent indicator of sterols in the microdomains.[44,45] Patch-like filipin-positive structures were present in all examined cells from pollen mother cells (PMCs) to GP (Figure 1 and Supporting Information Figure S2). These filipin-positive patches appeared to be clustered on one side of PMCs, and similar asymmetrical clusters were found far from the cell–cell boundary of dyads. The patches appeared to be redistributed uniformly in tetrads (Supporting Information Figure S2), and they became enriched on one side of microspores (MSs) (Supporting Information Figure S2). Then, the filipin-positive signals appeared in the periphery region and the aperture of bicellular pollen (BCP) and in the entire cell of immature tricellular (TCP) and mature pollen[38] with enrichment around the aperture (Figure 1 and Supporting Information Figure S2). The enriched patches became more obvious in the aperture of MP (Figure 1). Finally, the fluorescence intensity appeared polarized in the tips of bulges, with the morphologically visible prospective pollen tubes protruding out of the aperture and the side opposite against the newly born pollen tube of GP (Figure 1). MβCD treatment disrupted the filipin-positive signals in MP and GP (Figure 1). These data indicated microdomains present in pollen were selectively accumulated around the aperture and on the tip of bulges protruding from the aperture.

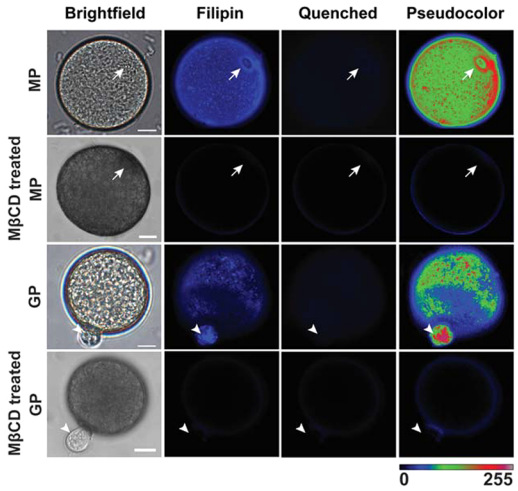

Figure 1. Distribution of sterols in rice mature and germinated pollen. Sterols were labeled with the fluorescent molecule, filipin. Pseudocolor images indicating the intensity of filipin-sterol fluorescence. Color bar represents the relative intensities from 0 to 255. MP, mature pollen; GP, germinated pollen. MβCD treated: filipin staining after MβCD treatment (60 mM MβCD, 50 mM Tris-HCl pH 7.5, 3 mM EDTA, complete protease inhibitor for 1h at 37 °C). Arrow: aperture. Arrow head: pollen tube. Bars = 10 μm.

Effect of MβCD treatment on sterols and membranes in pollen

Previous study showed that the pollen tube growth rate was significantly reduced by MβCD treatment.[46] Here, we directly treated MP with MβCD and prepared TMs from differentially treated pollen for further isolation of DRMs (Supporting

DOI: 10.1021/acs.jproteome.7b00852
J. Proteome Res. 2018, 17, 1532−1546

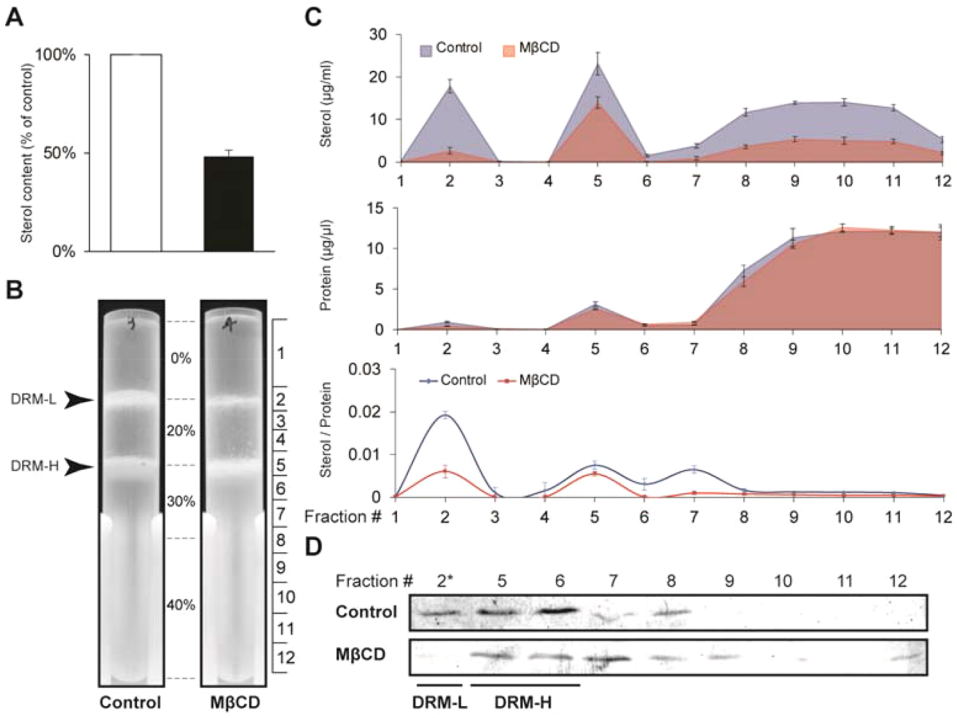

Figure 2. Isolation and protein and sterol examination of rice pollen DRMs. (A) Sterol removal efficiency detected in total membranes (TMs), $n = 3$. (B) Isolation of rice pollen DRMs by density gradient centrifugation. The gradient was collected into 12 fractions, from 1 to 12 as shown on the right side of the image. (C) Quantification of proteins and sterols in the 12 fractions, $n = 3$. (D) Immunoblot of flotillin-like protein. Equal amounts of proteins were loaded for fractions 2, 5, 6, and 7, which were 1/10 the amount of protein loaded in fractions 8 to 12.

Information Figure S3). MβCD treatment removed about 50% sterols from pollen TMs (Figure 2A). This depletion efficiency of sterols in our pollen samples is identical to that of MβCD-treated PMs from tobacco BY2 cells, and the removal of 50% sterols was sufficient to disrupt the BY2 microdomains.[47] Two coin-like DRM bands respective at 0%/20% (w/v) (low density DRM, DRM-L) and at 20%/30% (w/v) OptiPrep interface (high density DRM, DRM-H) were observed (Figure 2B). The two bands contained a small portion of loaded TM proteins, the majority of which were solubilized by Triton-X100 (Figure 2C). DRM-L had the highest ratio of sterol/protein, which is an index for microdomain enrichment[24] as compared to DRM-H and other fractions (Figure 2C). Western blot analysis showed that both DRM-L and DRM-H contained flotillin-like protein (Figure 2D), a rice homologue of flotilin proteins used as microdomain markers in different species,[24,48−50] and MβCD-mediated sterol depletion greatly decreased flotillin-like protein abundance in DRM-L and did not in DRM-H compared to respective controls (Figure 2D). The sterol-dependent abundance of proteins in DRM-L was identical to previous observations that membrane association of microdomain proteins is dependent on sterols in plant and animal cells,[31,32] thus indicating that microdomains were the main membrane moiety present in DRM-L fractions. Taken together, we identified microdomain-associated proteins using DRM-L by differential MβCD treatment.

Identification and quantification of proteins

We employed GeLC-MS and GeLC-MS/MS for the quantification and identification of proteins (Supporting Information Figure S3). The hydrophobicity of membrane proteins and interference from nonprotein membrane components make membrane proteomic research challenging.[51] The nonprotein components including lipids and pigments interfere with gel-based separation of membrane proteins, subsequent in-gel digestion, and mass spectrometry analysis.[52] To more efficiently dissolve DRM proteins and remove lipids and pigments, we have modified the method used for solubilizing and separating plant DRM proteins.[43] Major modifications included replacing sonic bath with sonic probe and carrying out reduction and alkylization during DRM protein preparation. Using this modified method, we successfully obtained highly reproducible 1D SDS-PAGE separation of membrane proteins in clear and regular bands with low background (Supporting Information Figure S4), indicating the modified method can efficiently solubilize membrane proteins and improve the resolution of SDS-PAGE.

We separated treated and control DRM samples with 5 replicates on one SDS-PAGE gel and horizontally divided the gel into 10 independent groups according to the molecular weight from top to bottom (Supporting Information Figure S3 and S4). Each group had 5 repeated treated and control samples, and quantification (LC-MS) and identification (LC-MSMS) were carried out group by group (Supporting Information Figure S3). LC-MS analysis revealed the good reproducibility among replicates (Supporting Information Figure S5 and S6). Because of the presence of isoforms derived from alternative splicing or post-translational modifications of a gene product, in GeLC-MS/MS analysis one protein might be identified and quantified repeatedly in several groups[53] (Supporting Information Table S1a). Combining all data, we identified 934 distinct proteins in total from DRM-L (Supporting Information Table S1b and Figure S7).

Among the 934 proteins, 682 (73.02%) had quantification information in at least one quantification group, of which only the peptide results with t test model $p < 0.05$ were used for median algorithm calculation (Supporting Information Table S1). 64.52% of the 682 proteins quantified were determined by more than one unique peptide (the coefficient of variance can be

DOI: 10.1021/acs.jproteome.7b00852
J. Proteome Res. 2018, 17, 1532−1546

calculated) (Supporting Information Table S1a), and the reliability of quantification results were validated with Western blotting examination of proteins (Figure 3). In order to evaluate

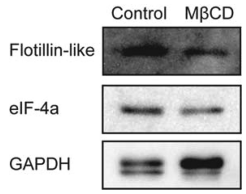

Figure 3. Immunoblot of three proteins in rice pollen DRM-Ls. Flotillin-like protein (BAD23328); eIF-4a, the eukaryotic initiation factor-4a (gil115444197); GAPDH, glyceraldehyde-3-phosphate dehydrogenase (gil115459078). 10 μg of proteins were loaded in each lane.

the label-free quantification results, we performed differential analysis using ratios (Control/Treatment, C/T) of all peptides (29044 in total). Statistical analysis of the lg (C/T) of root-mean-square, 90% confidence (RMS90) of the peptides showed the mean value of RMS90 peptides lg(C/T) is around 0.02 with the standard deviation (S.D.) of around 0.09. Two-times the SD distance from the mean value is generally considered as a significant threshold (Supporting Information Figure S8), which indicated here the cutoffs of significant fold change are 0.68 and 1.61. However, proteins with the fold change lower than 1.61 (eIF-4a, 1.37) or higher than 0.68 (GAPDH, 0.78) showed detectable changes in Western blots (Figure 3). This indicated the cutoff threshold determined by the statistical analysis of peptide ratios may have been too severe, which led to loss of some quantification information. Furthermore, one of the four identified flotillin homologues (Supporting Information Table S1) had quantification information with 1.50-fold down-regulation in treatment as compared with control, a fold change close to 1.61 (Row number: G8-155, Supporting Information Table S1a), and flotillin has been characterized as a microdomain marker in animal[48,49] and plant cells.[24,50] Taken together, we considered 1.50-fold change a reasonable cutoff to screen MβCD-sensitive proteins. If a protein identified in multiple groups had more than one quantification value, then it was classified according to the highest value; phosphatidylinositol-4-phosphate 5-kinase 4 was an example (Row number: G7-99, Table 1 and Supporting Information Table S2). This protein was identified in both G7 (G7-99) and G8 (G8-240) with the fold changes of 1.90 in G7 and 1.31 in G8; therefore, it was considered a MβCD-sensitive protein because the result indicated that at least one isoform of this protein could be recruited to lipid rafts (Supporting Information Table S1a). In total, among the 682 proteins quantified, 237 were identified as sterol-dependent proteins (SDPs) (fold change of C/T $\geq$ 1.50) (Supporting Information Table S2), which represented microdomain-associated proteins, and 445 were sterol-independent proteins (SIPs) (fold change of C/T < 1.50) (Supporting Information Table S1). The two data sets were used for further analysis.

Functional categories of proteins

According to functional annotation information in databases and homologue searches in NCBI, UniProt, ARAMEMNON, RGAP, TAIR, and SMART databases, we can assign the SDPs and SIPs into 10 functional groups: signal transduction, cell wall-related, membrane trafficking, transmembrane transport, redox and electron transport, cytoskeleton related, metabolism, protein synthesis, protein processing, and protein catabolism. Functionally unknown proteins and those not clearly assigned were organized into the "other" group (Figure 4 and Supporting Information Table S1b). A comparison showed the SDP data set had a higher proportion of proteins implicated in transmembrane transport, redox system and electron transport, and cytoskeleton, and to a lesser extent protein synthesis, protein processing, and protein catabolism than the SIP data set (Figure 4). The two data sets appeared have a similar proportion of proteins involved in signal transduction and membrane trafficking.

Because each category contained distinct protein families which further had distinct functional specificities, we further evaluated the distribution of distinct protein families in SDP and SIP data sets. The analysis clearly revealed that proteins of several categories showed preferred enrichment in SDP than SIP data sets (Figure 5). These proteins included (1) GTP-binding proteins and their regulators (such as ROP and its regulator RhoGAP) with the exception of Rab-related proteins, and almost all lipid signaling proteins; (2) the COPI coat proteins and exocytosis pathway proteins including Sec5, Exo70, and Sec1b, and adaptin family proteins; (3) actin binding proteins myosin, villin/gelsolin, and fimbrin 1 and tubulin proteins; (4) EMP70 proteins; and (5) V and P-ATPase proteins, calcium-transporting ATPases 9, and MFS transporters (Figure 5 and Supporting Information Table S1b). However, all members of the ABC transporter superfamily of proteins were in the SIP data set (Figure 5D and Supporting Information Table S1b). This finding is quite different from those observed in *Arabidopsis* suspension cells[32] which do not have cell polarity.[54,55] Several components of the mitochondrial respiratory chain were identified in DRMs and appeared to be sterol-dependent (Figure 5E), which could be related to the recently reported mitochondrial raft-like microdomains.[56,57] In addition, our data demonstrated that almost all ribosomal proteins identified were sterol-independent (SIP data set) (Figure 5F), which was consistent with the previous report that the ribosomal proteins identified in DRMs were not sensitive to MβCD-mediated sterol disruption in *Arabidopsis* suspension cells.[32] Despite this, ribosomal proteins have been widely identified in DRMs and PM from a diverse set of other species.[43,58−60] This further indicated that differential treatment of MβCD is a useful approach to identify raft-associated proteins from DRMs.

Rice mature pollen has a more similar microdomain proteome with HeLa cells than *Arabidopsis* suspension cells

To better assess how effective our technique is and better understand the composition of the rice pollen microdomain proteome, we compared the evolutionary conserved (between plant and animal kingdoms) proteins from the pollen microdomain proteome to those from *Arabidopsis* suspension cells and Hela cells, which were also identified using the MβCD depletion strategy.[31,32] Surprisingly, although rice cells are more evolutionarily closer to *Arabidopsis* cells than HeLa cells, this is not the case in terms of composition and sterol-sensitivity for these identified evolutionary conserved proteins. In fact, rice pollen and HeLa cell displayed much more similarity to each other in both composition and sterol-sensitivity despite being more evolutionarily divergent (Figure 6). HeLa cell is the most popular human immortal model cell line used in research and was derived from cervical cancer cells. During the EMT processes, it lost the typical characteristics of epithelial cell and gained higher migratory and invasive properties,[61] and its polarity was switched from apical-basal to front-rear direction.[34] Since HeLa cells are still polarized cells after EMT while the *Arabidopsis* cells are

DOI: 10.1021/acs.jproteome.7b00852
J. Proteome Res. 2018, 17, 1532−1546

Table 1. Signal Transduction Proteins in the SDP Dataset[a]

Accession	Name	Rows	Peptides	SC	Median (C:T)	CV [%] (C:T)
gil31126785	WD repeat G protein beta family	G2-144	2	5.8	3.65	0.00
		G6-133	4	13.4	1.57	15.15
gil38175440	Dynamin homologue	G5-42	7	13.6	1.51	9.13
		G7-66	9	20.5	1.69	0.00
gil18071348	Dynamin-type large GTPase	G6-63	9	27.5	1.56	9.77
gil218188848	Dynamin-type large GTPase	G6-151	4	8.7	1.51	4.93
gil115456231	RAB8C	G2-50	4	25.7	1.91	0.00
gil115443865	Rop subfamily protein	G1-181	3	18.3	1.67	0.00
gil218192466	RhoGAP	G6-240	1	2.6	1.78	0.00
gil38344114	ARF-GEF	G2-67	3	6.5	2.08	0.00
		G9-165	3	1.9	1.63	0.00
gil20161472	ADP-ribosylation factor	G1-36	9	25.8	1.85	12.25
		G3-102	6	25.8	1.97	12.10
		G4-124	5	25.8	1.85	18.70
		G5-161	2	12.5	1.58	0.00
		G6-143	2	20.2	1.96	0.00
		G8-226	1	5.9	1.73	0.00
		G10-8	11	25.8	1.92	5.56
gil115475543	ADP-ribosylation factor 3	G10-147	2	14.8	1.85	0.00
gil108711707	ADP-ribosylation factor	G2-38	7	50.0	3.33	18.31
gil125560755	Arf-type small GTPase	G10-175	1	20.2	1.85	0.00
gil52353766	Phospholipase D	G2-70	4	8.6	2.67	0.00
gil18765900	Phospholipase D beta 2	G3-127	4	10.5	1.51	4.67
gil77548655	Phosphatidylinositol-4-phosphate 5-kinase 4	G7-99	4	8.5	1.90	0.00
gil77548643	Phosphatidylinositol-4-phosphate 5-kinase 4	G7-91	5	11.5	1.90	0.00
gil62733536	Phosphatidylinositol 3- and 4-kinase	G2-16	10	11.0	2.04	7.85
gil115479967	Type II inositol-1,4,5-trisphosphate 5-phosphatase 12	G4-168	4	4.8	1.54	21.87
gil115446675	Phosphoinositide 5-phosphatase	G6-121	3	6.9	1.54	6.84
gil115485223	Phosphoinositide 5-phosphatase	G2-2	26	46.9	1.86	8.91
		G5-5	22	45.9	1.63	9.45
		G6-32	15	31.7	1.62	17.40
		G9-13	11	25.3	1.50	5.42
gil115443641	Pleckstrin homology-type domain containing protein	G2-46	3	12.6	1.89	0.00
		G5-85	4	10.0	1.52	1.60
		G6-168	3	7.8	1.65	0.00
		G7-75	6	12.9	1.67	0.00
		G8-44	7	11.8	1.50	3.16
gil47497419	Vacuolar protein sorting 13C protein-like	G2-63	4	2.0	1.88	15.79
gil115438829	STE-type protein kinase	G7-106	5	11.4	1.62	0.00
gil115478094	Protein kinase domain containing protein	G6-205	2	20.1	2.11	1.50
gil125525877	Leucine-rich repeat receptor-like protein kinase	G1-205	1	9.1	1.62	0.00
gil31712071	Protein phosphatase 2A regulatory subunit B′	G5-64	4	17.2	1.77	0.00
gil115478158	Protein phosphatase 2A A subunit	G6-245	2	9.0	2.05	0.00
gil21952835	Calcineurin-like phosphoesterase	G1-129	5	7.9	1.90	0.00
gil115448739	Annexin p35, similar	G2-116	2	15.6	1.75	0.00
gil115464965	Hexokinase 1	G2-53	3	19.7	2.26	0.00
		G5-3	29	72.8	1.98	12.34
gil115446017	Fasciclin-like arabinogalactan protein	G1-187	2	15.5	1.65	0.00
		G2-135	1	10.3	4.16	0.00
		G3-198	3	15.5	1.75	0.00
		G6-260	1	10.3	1.83	0.00
		G7-120	3	10.3	1.88	0.00

[a]Rows: ranks of the specified proteins relative to all other proteins in the list of detected proteins (The serial numbers in the original analysis group). Peptides, the numbers of unique peptides. SC, Sequence coverage. Median (C:T), Median of control/treatment ratios (peptides). CV, Coefficient of Variance. Detailed information in Supporting Information Table S2.

nonpolarized, this result suggested that the microdomain-mediated mechanisms for cell polarity might have similarity between plant and animal cells.

Subcellular localization and lipid modification analysis of proteins

According to annotations from the RGAP and TAIR databases, 84.39% (200/237) of SDPs and 88.09% (392/445) of SIPs were

DOI: 10.1021/acs.jproteome.7b00852
J. Proteome Res. 2018, 17, 1532−1546

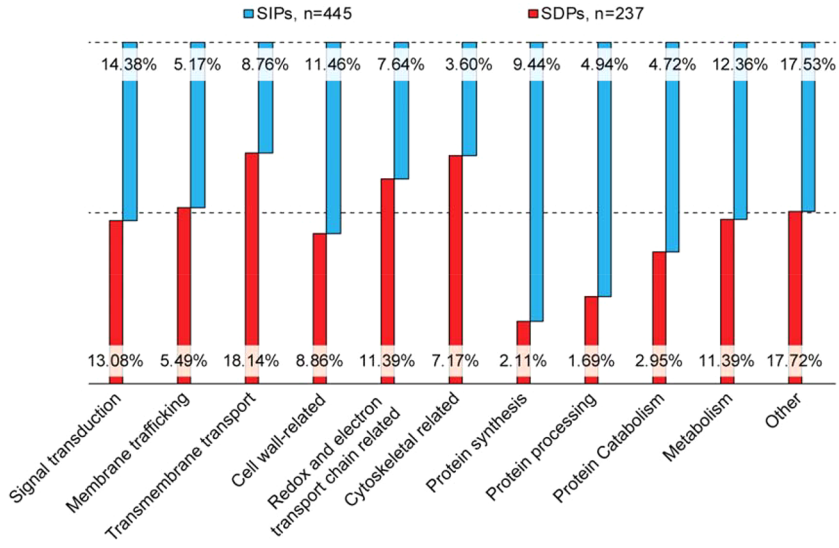

Figure 4. Functional classification of sterol-dependent proteins (SDPs) and sterol-independent proteins (SIPs). The 100% stacked column chart shows the percentage of SIPs and SDPs in each functional group.

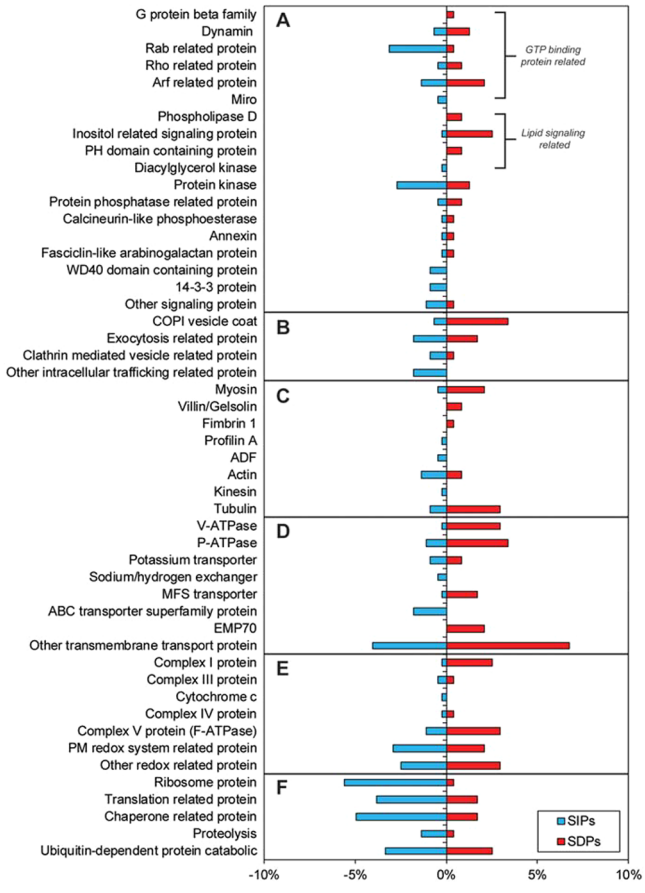

Figure 5. Protein distribution of main protein families in SDP and SIP data sets. (A) Signal transduction. (B) Membrane trafficking. (C) Cytoskeleton. (D) Transmembrane transport. (E) Redox and electron transport chain related. (F) Protein synthesis, processing and catabolism.

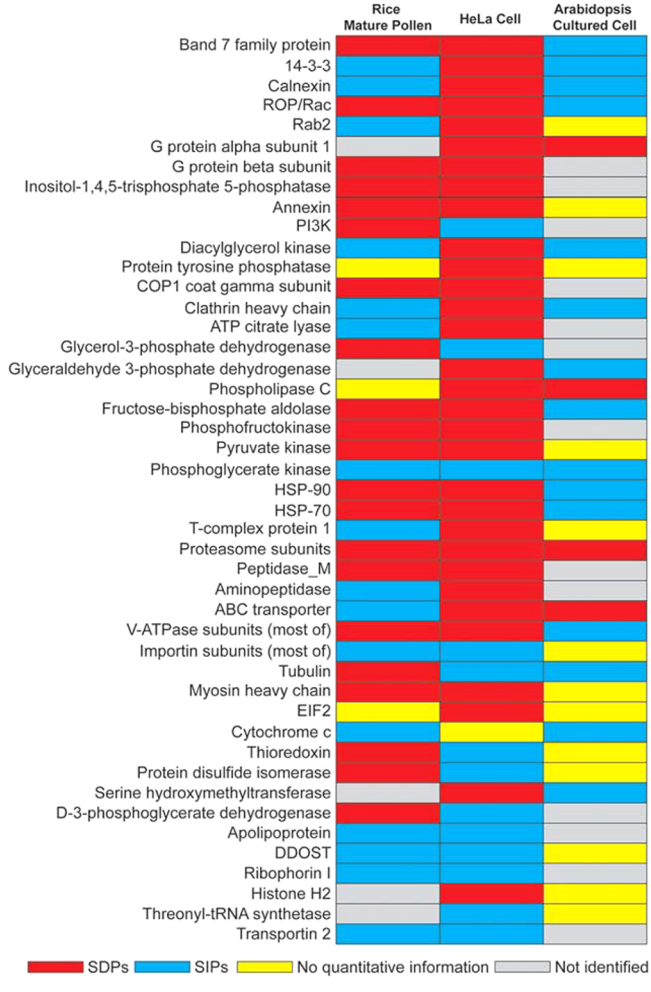

Figure 6. Comparison of SDPs and SIPs from rice mature pollen, HeLa cells, and *Arabidopsis* cultured suspension cells (ribosomal proteins not included). Only the proteins conserved between either rice and human or *Arabidopsis* and human were included.

annotated as membrane proteins (Figure 7 and Supporting Information Table S1b). 52.00% of the 200 SDP membrane proteins were PM-related (PM, cell wall), and others were predicted to reside in the endoplasmic reticulum (ER), Golgi body, and vacuoles (Figure 7A and Supporting Information Table S1b). The result suggested that besides a preferred

DOI: 10.1021/acs.jproteome.7b00852
J. Proteome Res. 2018, 17, 1532−1546

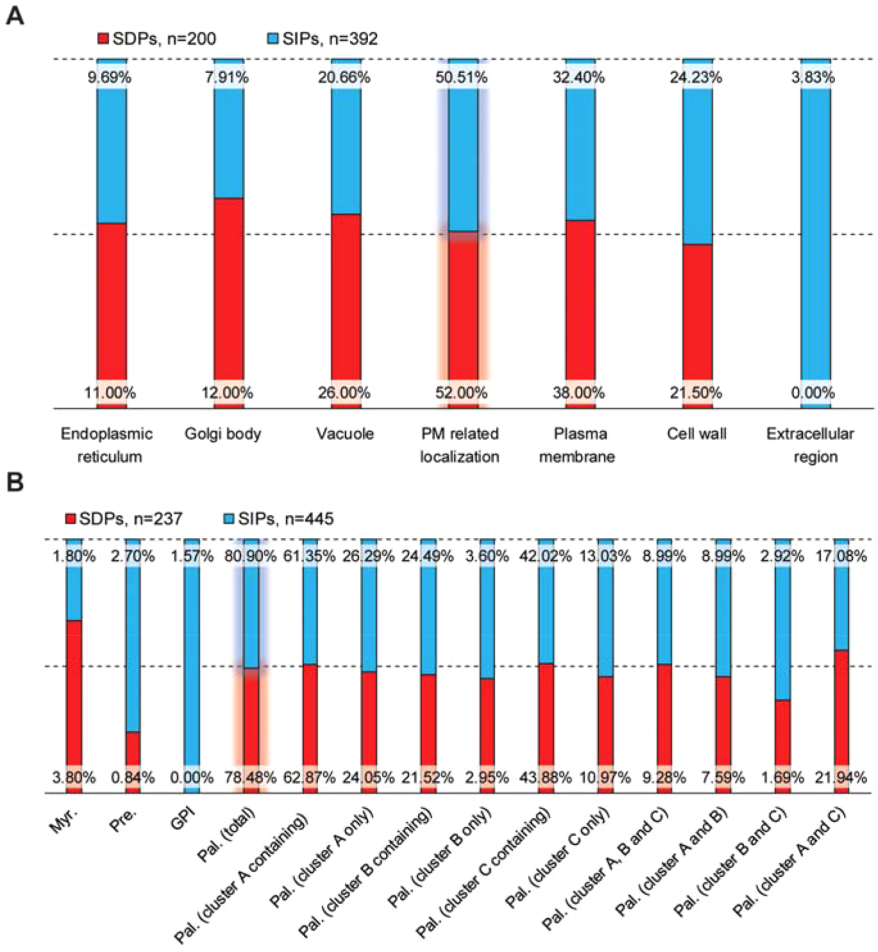

Figure 7. Subcellular localization and lipid modifications of SDPs and SIPs. (A) Comparison of the subcellular localization of SDPs and SIPs. PM-related localization includes plasma membrane, cell wall, and the extracellular region. (B) Comparison of lipid modifications on SDPs and SIPs. Myr., myristoylation; Pre., prenylation; GPI, glycosylphosphatidylinositol anchor; Pal., palmitoylation; cluster A-C, subtypes of palmitoylation.

presence in the PM, lipid rafts were also present in the endomembrane system, which appeared to be associated with the difference in sterol and sphingolipid concentration within these membranes: high in PM and low in ER and Golgi body.[16,62] SIPs were annotated localized in these subcellular compartments with a lower relative percentage of proteins in ER, Golgi body, vacuole, and PM than SDPs (Figure 7A). Unexpectedly, we found all of extracellular proteins, which are considered associated with the outer leaflet of the PM, were in the SIP but not in the SDP data set (Figure 7A), thus implying that the rice pollen PM inner leaflet-localized proteins should be more sensitive to sterol disruption than outer leaflet proteins.

Protein lipid modifications[62] including S-palmitoylation, N-myristoylation, prenylation, and GPI-anchors are important determinants for the association of soluble proteins to the PM or microdomains, and they are possibly involved in coordinating the localization of both soluble and integral proteins between raft and nonraft domains.[63] Our prediction showed 80.06% of the 682 quantitative DRM proteins had putative sites for S-pamitorylation, 2.35% for N-myristoylation, 2.05% for prenylation, and 0.88% for the GPI-anchor. Among SDPs, 78.48% were predicted to have a putative site for S-pamitoylation, 3.80% for N-myristoylation, and 0.84% for prenylation (Figure 7B and Supporting Information Table S1b), which is comparable to the predicted modifications of SIPs. Compared with the SIP data set, the SDP data set had a larger number of proteins with N-myristoylation sites (3.80% vs 1.80%) and clusters A and C of S-palmitoylation sites (21.94% vs 17.08%), a smaller number of proteins with prenylation (0.84% vs 2.70%) and clusters B and C of S-palmitoylation sites (1.69% vs 2.92%), and none with GPI-anchor sites (0% vs 1.57%) (Figure 7B). This implies that proteins with N-myristoylation or S-palmitoylation at clusters A and C were preferentially localized to microdomains in pollen.

Immunogold localization of flotillin-like protein displays nonhomogeneous cluster patterns

Currently, electron microscopy is the most conclusive method for the observation of nanoscale microdomains. To further verify the identification of microdomain-associated proteins, we performed immunogold labeling of a flotillin-like protein to determine its localization (Figure 8). Flotillin proteins have been used as a marker of microdomains in animal and plant cells.[24,48−50] In pollen labeled with an antibody against flotillin-like protein, we observed clustered gold particles with some scattered signals (Figure 8D−F and Supporting Information Table S3). This unique clustered distribution pattern is comparable with that of other microdomains markers, such as remorin[64] and PtdIns(4,5)P2[65] and represents characteristics of microdomains. The clusters increase in size and number as pollen develops, and they reached a maximum size and number in mature pollen. However, the ratio between clustered and scattered gold particles alternately oscillated during pollen

DOI: 10.1021/acs.jproteome.7b00852
J. Proteome Res. 2018, 17, 1532−1546

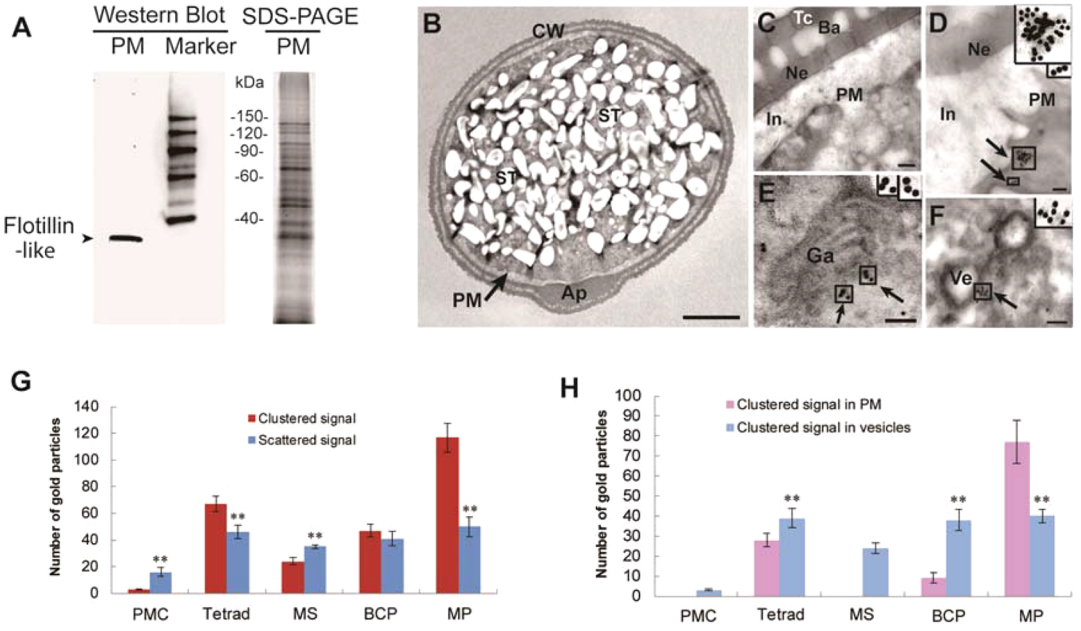

Figure 8. Immunogold labeling and localization of flotillin-like protein in rice mature pollen. (A) Western blot examination of flotillin-like protein in plasma membrane (PM) (10 μg proteins loaded). (B–F) Immunogold labeling of flotillin-like protein. (B) Electron micrograph depicting a full-view section of mature rice pollen. Bar = 5 μm. CW, cell wall; Ap, aperture; ST, starch granule. (C) Preimmune serum controls showing no gold signal in the cell. Bar = 200 nm. Tc, tectum; Ba, bacula; Ne, nexine; In, intine. (D) Clusters (minimum of 3 gold particles) in the PM (arrows), indicative of "lipid rafts". Bar = 100 nm. (E) Clusters in the Golgi apparatus (arrows). Bar = 100 nm. Ga, Golgi apparatus. (F) Clusters in vesicles (arrows). Bar = 100 nm. Ve, vesicle. Insets in D–F: High magnification micrographs showing clusters. (G) Statistical data representing the clusters already present in PMC and the maximum number of clusters in mature pollen (n = 5). (H) Statistical data indicating that mature pollen has a higher proportion of clusters in the PM than in vesicles (n = 5).

development (Figure 8G and Supporting Information Table S3a). We further analyzed the distribution of the clusters in the PM and endomembrane structures. More clusters in endomembrane structures such as the Golgi apparatus and intracellular vesicles were detected in PMCs as they transitioned to BCP, but the clusters were more apparent in the PM of MP (Figure 8H and Supporting Information Table S3b). Taken together, these results clearly visualized microdomains in pollen and show a clear shift between BCP and MP.

DISCUSSION

Sterol-rich membrane microdomains, the liquid-ordered membrane islets, are involved in lots of important biological processes by serving as functional molecules organizing centers and directional membrane trafficking logistic carriers.[15] Here we showed that filipin-positive patches began appearing around the aperture in bicellular pollen and became enriched in the aperture of mature pollen and the tip of newborn pollen tubes protruding from the aperture; MβCD-mediated disruption of sterols led to loss of the filipin-positive patches. The asymmetric enrichment of microdomains around the aperture and in subsequent tips of the newborn pollen tube indicates that pollen establishes polarity cues for future pollen tube initiation during pollen maturity, thus suggesting that microdomains serve as an upstream player of pollen polarity. However, a question that remains to be addressed is why microdomains become enriched around the aperture. Studies on aperture development suggested that the position of apertures usually was at the last cytoplasmic contact points between the future microspores.[66] The plasmodesmata which mediates the cell–cell cytoplasmic communication in plants also had enriched microdomains.[64,67] It will be very interesting to further dissect why microdomains are enriched around the aperture.

Interestingly, besides enrichment in the aperture and the tip of newly born pollen tubes, the filipin-positive patches changed dynamically during pollen development and germination: the patches were in the periphery region in PMCs, asymmetrically clustered far from the cell–cell boundary of dyads, clustered in entire tetrads, asymmetrically clustered in one side of MS, in the periphery region of BCP, in the entire cell of TCP and MP, and in the side opposite against the newly born pollen tube of GP. The dynamic changes were possibly associated with unique developmental events of pollen, such as nuclei changes in PMCs and MS polarity and vacuolization and cell division in BCP, although the biological importance of the microdomains needs further investigation.

Furthermore, we revealed 237 sterol-dependent proteins from DRMs by use of MβCD-based quantitative proteomic approaches, which allow discrimination between proteins copurifying in the DRM fraction and true proteins dependent on sterol-rich membrane regions.[32] Our immunogold analysis of flotillin-like protein, a representative sterol-dependent protein, revealed a clustered distribution in the membrane. The clustered distribution in the membrane is the characteristic of microdomains.[28,29] Thus, the 237 sterol-dependent proteins in sterol-rich membrane regions represent micordomain-associated proteins.

The pollen microdomain-associated proteome includes most known key players of the regulating network of tip growth (Table 1 and Figure 9), including the central player of the network, ROP, and its negative regulator RopGAP (Figure 9A), most of the key phospholipid-related enzymes, and calcium-ATPases. The apical domain-localized ROP regulates F-actin dynamics in

DOI: 10.1021/acs.jproteome.7b00852
J. Proteome Res. 2018, 17, 1532–1546

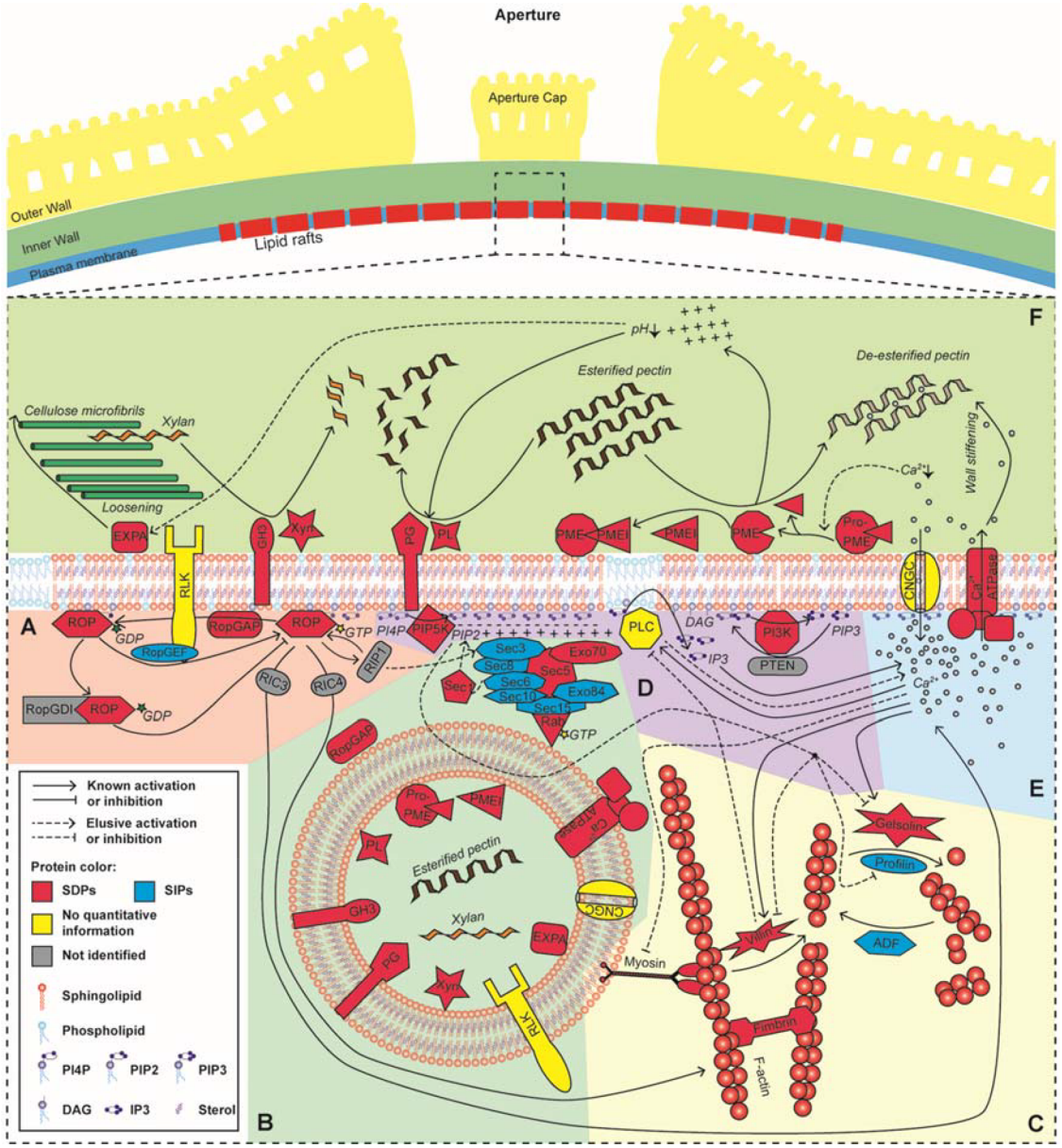

Figure 9. Model of the proposed sterol-rich membrane microdomain-mediated polarity cues established in mature pollen. During pollen development, microdomain rafts are enriched around the germination aperture. The microdomains contain most of the known key players of tip growth, singling out networks, newly identified signaling molecules, and proteins in other functional categories. The pre-established polarity cues support future tip growth. (A) ROP pathways (light red area) with the known positive and negative regulations of ROP shown, and receptor-like kinases (RLKs) that potentially act upstream. ROP, Rho-related small GTPase from plant; RopGAP, Rop GTPase-activating protein; RopGEF, Rop guanine nucleotide exchange factor; RopGDI, Rop guanine nucleotide dissociation inhibitor; RIC, CRIB motif-containing protein; RIP1, ROP interactive partner 1. (B) Exocytic vesicle and related proteins (light green area), showing the potential tip targeting secretory complexes, vesicle, and cargos. Sec, secretion (related proteins); Exo, Exocyst complex component. (C) F-actin dynamics (light yellow area), showing the potential assembly, disassembly, and motility of F-actin under the aperture. ADF, Actin-depolymerizing factor. (D) Phospholipid signaling pathways (light purple area), showing the catalytic relationship among different key players in these pathways. PIP5K, phosphatidylinositol-4-phosphate 5-kinases; PLC, phospholipase C; PI3K, phosphatidylinositol-4,5-bisphosphate 3-kinase; PTEN, phosphatase and tensin homologue; CNGC, calcium-permeable cyclic nucleotide-gated channel. (E) Efflux and influx of Ca^{2+} (light blue area). (F) Cell wall remodeling (olive green area), showing the proteins involved in pollen cell wall dynamics. EXPA, expansin; GH3, glycosyl hydrolase family 3 protein; Xyn, xylanase; PG, polygalacturonase; PL, pectate lyase; PME, pectin methylesterase; PMEI, PME inhibitor.

the apical cytoplasm via downstream effectors RIC3 and RIC4 and/or tip-focused Ca^{2+} gradient.[8,68] The phospholipid-related enzymes modulate the synthesis and dynamic equilibrium of phosphatidylinositol 4,5-bisphosphate (PIP2), diacylglycerol (DAG), IP3, and PIP3 for tip growth.[11,69,70] Studies showed that PIP5K4 as well as PIP2 and DAG were localized to the subapical and/or apical PM.[11,70] The phospholipid molecules regulate F-actin dynamic directly or via a tip-focused Ca^{2+} gradient[8] and could provide a docking signal for exocyst complexes via electrostatic interactions[71−73] (Figure 9B−E). Thus, ROP and phospholipid signals co-orchestrate F-actin dynamics and polarized vesicular transport required for tip growth by supplying new PM and wall materials.[8]

The pollen microdomain-associated proteome also contained the actin-binding proteins (ABPs) gelsolin, villin, fimbrin, and myosin (Figure 9C) which mediate F-actin assembly, dis-

DOI: 10.1021/acs.jproteome.7b00852
J. Proteome Res. 2018, 17, 1532−1546

assembly, and bundling or provide motility during actin-based transport. Besides the actin-based motor protein myosin, the exocyst subunits Exo70 and Sec5 are also found to belong to SDPs (Figure 9B). Exo70 together with Sec3 are involved in the navigation of the final cargo delivery position on apex PM (Figure 9B),[71] and they are localized in the tips of growing pollen tubes.[74] Additionally, Sec1 and Rab8C identified in pollen microdomains (Supporting Information Table S1) were previously implicated in the fusion of exocytic vesicles with the PM in yeast and animal cells[75] and vesicular transport between the trans-Golgi network and PM in animal cells.[38,76] Interestingly, among the 19 Rab proteins identified in the pollen DRMs, only Rab8 was in the pollen microdomain-associated proteome (Supporting Information Table S2). In animal cell lines, Rab8 turnover controlled the cell polarization.[77] One of the most important materials delivered by exocytic vesicles is polysaccharide building blocks and proteins for the cell wall (Figure 9B and F).[8] The pollen microdomain-associated proteome included cell wall plasticity-related enzymes such as PMEs, PMEI, pectate lyase (PL), polygalacturonase (PG), glycosyl hydrolase family 3 protein (GH3), xylanase (Xyn), and expansin (EXPA) (Supporting Information Table S1 and Figure 9F). PMEs de-esterify esterified pectin, which makes the cell wall more rigid at the subapical region, while PMEI inhibits the activity of PME, which keeps the cell wall more flexible at the apex.[78] PL and PG function in degrading pectin,[79,80] and GH3 and Xyn, in degrading xylan.[81] EXPA plays roles in loosening cellulose microfibrils.[82] Collectively, these results demonstrated that in mature pollen, microdomains are enriched around the aperture, the future pollen tube initiation sites, and have recruited key molecules involved in signaling and functional proteins required for polar cell growth. Thus, our results suggest that pollen has established polarity cues during maturation and microdomains could be an upstream player of pollen polarization. Because of the comparisons of evolutionary conserved proteins among microdomain-associated proteomes of mature rice pollen and because *Arabidopsis* suspension cell and front−back polarized HeLa cell show that the pollen microdomain-associated proteome is more similar to those found in front−back polarized HeLa cells than *Arabidopsis* suspension cells, it is plausible that the underlying mechanisms of polarity establishment are evolutionarily convergent across plant and mammalian cells.

Although most of the important players of known tip growth pathways of pollen tubes were found in the rice pollen microdomain proteome, they still only weight a small portion of the pollen microdomain proteome. The remaining proteins in this proteome might be potential new players in the known pathways or mediate tip growth via present unknown pathways. For example, the fasciclin (FAS1) domain of the fasciclin-like arabinogalactan protein identified in this proteome is a very ancient domain common from eukaryotic to prokaryotic cells.[83,84] FAS1 domain contained proteins are involved in axonal guidance in animals and in cotton fiber initiation/elongation in plants.[85,86] So, our data can serve as a powerful resource to advance future studies dissecting the molecular mechanisms for the establishment and maintenance of cell polarity.

CONCLUSIONS

Sterol-rich membrane microdomains were dynamic during pollen development, and became enriched around the aperture from the BCP stage and maintained this localization pattern until germination. We identified 237 microdomain-associated proteins, which can be divided into different functional categories and included a large subset of signaling molecules. The proteome covered most of the known core players of the tip growth regulation network, and it shows similarities to that of polarized human Hela cells compared to nonpolarized *Arabidopsis* suspension cells. Taken together, these indicate that polarity cues are likely established during pollen maturity via microdomain-based mechanisms, far before pollen germination. Most of the proteins in the pollen microdomain-associated proteome have not been extensively investigated or have yet to be identified. Thus, this work provides a novel breadth of knowledge and can serve as a powerful resource to advance future studies dissecting the molecular mechanisms for the establishment and maintenance of cell polarity.

ASSOCIATED CONTENT

Supporting Information

The Supporting Information is available free of charge on the ACS Publications website at DOI: 10.1021/acs.jproteome.7b00852.

(Figure S1) Flotillin-like protein antibody preparation. (Figure S2) Distribution of sterols in developing pollen. (Figure S3) Work flow used to identify sterol-rich membrane microdomain-associated proteins of mature rice pollen. (Figure S4) SDS-PAGE separation of proteins from rice pollen DRM-Ls. (Figure S5) Representative images for protein identification and quantification with ESI-Qq-TOF mass spectrometer. (Figure S6) Comparisons of the chromatograph profiles among these duplicates (from analysis group 1 to 10). (Figure S7) MS/MS fragmentation spectra of peptides, which led to identification of a protein by only itself. (Figure S8) Volcano plot depicting the quantification results of label-free peptides. (Table S3) Statistical analysis of gold particle distribution in developing rice pollen (PDF)

(Table S1) Quantification and annotation of all identified proteins (XLSX)

(Table S2) List of 237 proteins of the sterol dependent protein data set (XLSX)

AUTHOR INFORMATION

Corresponding Author

*E-mail, twang@ibcas.ac.cn; Phone, 0086-10-62836210.

ORCID

Tai Wang: 0000-0003-2752-697X

Present Address

⊥(B.H.) Department of Molecular Physiology and Biophysics, Vanderbilt University, USA.

Author Contributions

†B.H. and N.Y. contributed equally to this work

Notes

The authors declare no competing financial interest.

ACKNOWLEDGMENTS

This work was supported by Chinese Ministry of Science and Technology (grant no. 2013CB945101) and Chinese Academy of Sciences (grant no. KSCX2-YW-N-026). The authors thank Dr. Qing Zhang from Bruker Daltonics for instrumental support

DOI: 10.1021/acs.jproteome.7b00852
J. Proteome Res. 2018, 17, 1532−1546

and Dr. Courtney Copeland from Vanderbilt University (TN, USA) for help with manuscript editing.

REFERENCES

(1) Schmidt, A.; Schmid, M. W.; Grossniklaus, U. Plant germline formation: common concepts and developmental flexibility in sexual and asexual reproduction. *Development* **2015**, *142* (2), 229−41.
(2) Hafidh, S.; Fíla, J.; Honys, D. Male gametophyte development and function in angiosperms: a general concept. *Plant Reprod.* **2016**, *29* (1−2), 31−51.
(3) Blackmore, S.; Wortley, A. H.; Skvarla, J. J.; Rowley, J. R. Pollen wall development in flowering plants. *New Phytol.* **2007**, *174* (3), 483−98.
(4) Dresselhaus, T.; Sprunck, S.; Wessel, G. M. Fertilization Mechanisms in Flowering Plants. *Curr. Biol.* **2016**, *26* (3), R125−39.
(5) Geldner, N. Cell polarity in plants: a PARspective on PINs. *Curr. Opin. Plant Biol.* **2009**, *12* (1), 42−8.
(6) Dettmer, J.; Friml, J. Cell polarity in plants: when two do the same, it is not the same.. *Curr. Opin. Cell Biol.* **2011**, *23* (6), 686−96.
(7) Qin, Y.; Dong, J. Focusing on the focus: what else beyond the master switches for polar cell growth? *Mol. Plant* **2015**, *8* (4), 582−94.
(8) Guan, Y.; Guo, J.; Li, H.; Yang, Z. Signaling in pollen tube growth: crosstalk, feedback, and missing links. *Mol. Plant* **2013**, *6* (4), 1053−64.
(9) Hwang, J. U.; Wu, G.; Yan, A.; Lee, Y. J.; Grierson, C. S.; Yang, Z. Pollen-tube tip growth requires a balance of lateral propagation and global inhibition of Rho-family GTPase activity. *J. Cell Sci.* **2010**, *123* (Pt 3), 340−50.
(10) Hwang, J. U.; Vernoud, V.; Szumlanski, A.; Nielsen, E.; Yang, Z. A tip-localized RhoGAP controls cell polarity by globally inhibiting Rho GTPase at the cell apex. *Curr. Biol.* **2008**, *18* (24), 1907−16.
(11) Helling, D.; Possart, A.; Cottier, S.; Klahre, U.; Kost, B. Pollen tube tip growth depends on plasma membrane polarization mediated by tobacco PLC3 activity and endocytic membrane recycling. *Plant Cell* **2006**, *18* (12), 3519−34.
(12) Samaj, J.; Müller, J.; Beck, M.; Böhm, N.; Menzel, D. Vesicular trafficking, cytoskeleton and signalling in root hairs and pollen tubes. *Trends Plant Sci.* **2006**, *11* (12), 594−600.
(13) Lorent, J. H.; Levental, I. Structural determinants of protein partitioning into ordered membrane domains and lipid rafts. *Chem. Phys. Lipids* **2015**, *192*, 23−32.
(14) Nyholm, T. K. Lipid-protein interplay and lateral organization in biomembranes. *Chem. Phys. Lipids* **2015**, *189*, 48−55.
(15) Diaz-Rohrer, B.; Levental, K. R.; Levental, I. Rafting through traffic: Membrane domains in cellular logistics. *Biochim. Biophys. Acta, Biomembr.* **2014**, *1838* (12), 3003−3013.
(16) Lingwood, D.; Simons, K. Lipid rafts as a membrane-organizing principle. *Science* **2010**, *327* (5961), 46−50.
(17) Kamiguchi, H. The region-specific activities of lipid rafts during axon growth and guidance. *J. Neurochem.* **2006**, *98* (2), 330−5.
(18) Wen, Z.; Zheng, J. Q. Directional guidance of nerve growth cones. *Curr. Opin. Neurobiol.* **2006**, *16* (1), 52−8.
(19) Wachtler, V.; Rajagopalan, S.; Balasubramanian, M. K. Sterol-rich plasma membrane domains in the fission yeast Schizosaccharomyces pombe. *J. Cell Sci.* **2003**, *116* (Pt 5), 867−74.
(20) Nichols, C. B.; Fraser, J. A.; Heitman, J. PAK kinases Ste20 and Pak1 govern cell polarity at different stages of mating in Cryptococcus neoformans. *Mo.l Biol. Cell.* **2004**, *15* (10), 4476−89.
(21) Bagnat, M.; Simons, K. Cell surface polarization during yeast mating. *Proc. Natl. Acad. Sci. U. S. A.* **2002**, *99* (22), 14183−8.
(22) Martin, S. W.; Konopka, J. B. Lipid raft polarization contributes to hyphal growth in Candida albicans. *Eukaryotic Cell* **2004**, *3* (3), 675−84.
(23) Ovecka, M.; Berson, T.; Beck, M.; Derksen, J.; Samaj, J.; Baluska, F.; Lichtscheidl, I. K. Structural sterols are involved in both the initiation and tip growth of root hairs in Arabidopsis thaliana. *Plant Cell* **2010**, *22* (9), 2999−3019.
(24) Liu, P.; Li, R. L.; Zhang, L.; Wang, Q. L.; Niehaus, K.; Baluska, F.; Samaj, J.; Lin, J. X. Lipid microdomain polarization is required for NADPH oxidase-dependent ROS signaling in *Picea meyeri* pollen tube tip growth. *Plant J.* **2009**, *60* (2), 303−13.
(25) Men, S.; Boutté, Y.; Ikeda, Y.; Li, X.; Palme, K.; Stierhof, Y. D.; Hartmann, M. A.; Moritz, T.; Grebe, M. Sterol-dependent endocytosis mediates post-cytokinetic acquisition of PIN2 auxin efflux carrier polarity. *Nat. Cell Biol.* **2008**, *10* (2), 237−44.
(26) Sorek, N.; Segev, O.; Gutman, O.; Bar, E.; Richter, S.; Poraty, L.; Hirsch, J. A.; Henis, Y. I.; Lewinsohn, E.; Jürgens, G.; Yalovsky, S. An S-acylation switch of conserved G domain cysteines is required for polarity signaling by ROP GTPases. *Curr. Biol.* **2010**, *20* (10), 914−20.
(27) Tanner, W.; Malinsky, J.; Opekarova, M. In plant and animal cells, detergent-resistant membranes do not define functional membrane rafts. *Plant Cell* **2011**, *23* (4), 1191−3.
(28) Mongrand, S.; Stanislas, T.; Bayer, E. M.; Lherminier, J.; Simon-Plas, F. Membrane rafts in plant cells. *Trends Plant Sci.* **2010**, *15* (12), 656−63.
(29) Malinsky, J.; Opekarova, M.; Grossmann, G.; Tanner, W. Membrane microdomains, rafts, and detergent-resistant membranes in plants and fungi. *Annu. Rev. Plant Biol.* **2013**, *64*, 501−29.
(30) McGuinn, K. P.; Mahoney, M. G. Lipid rafts and detergent-resistant membranes in epithelial keratinocytes. *Methods Mol. Biol.* **2014**, *1195*, 133−44.
(31) Foster, L. J.; De Hoog, C. L.; Mann, M. Unbiased quantitative proteomics of lipid rafts reveals high specificity for signaling factors. *Proc. Natl. Acad. Sci. U. S. A.* **2003**, *100* (10), 5813−8.
(32) Kierszniowska, S.; Seiwert, B.; Schulze, W. X. Definition of Arabidopsis sterol-rich membrane microdomains by differential treatment with methyl-beta-cyclodextrin and quantitative proteomics. *Mol. Cell. Proteomics* **2009**, *8* (4), 612−23.
(33) Cheung, A. Y.; Wu, H. M. Structural and signaling networks for the polar cell growth machinery in pollen tubes. *Annu. Rev. Plant Biol.* **2008**, *59*, 547−72.
(34) Lee, M. Y.; Shen, M. R. Epithelial-mesenchymal transition in cervical carcinoma. *Am. J. Transl. Res.* **2012**, *4* (1), 1−13.
(35) Wei, L. Q.; Xu, W. Y.; Deng, Z. Y.; Su, Z.; Xue, Y.; Wang, T. Genome-scale analysis and comparison of gene expression profiles in developing and germinated pollen in Oryza sativa. *BMC Genomics* **2010**, *11*, 338.
(36) Itoh, J.; Nonomura, K.; Ikeda, K.; Yamaki, S.; Inukai, Y.; Yamagishi, H.; Kitano, H.; Nagato, Y. Rice plant development: from zygote to spikelet. *Plant Cell Physiol.* **2005**, *46* (1), 23−47.
(37) Kerim, T.; Imin, N.; Weinman, J. J.; Rolfe, B. G. Proteome analysis of male gametophyte development in rice anthers. *Proteomics* **2003**, *3* (5), 738−51.
(38) Huber, L. A.; Pimplikar, S.; Parton, R. G.; Virta, H.; Zerial, M.; Simons, K. Rab8, a small GTPase involved in vesicular traffic between the TGN and the basolateral plasma membrane. *J. Cell Biol.* **1993**, *123* (1), 35−45.
(39) Dai, S.; Chen, T.; Chong, K.; Xue, Y.; Liu, S.; Wang, T. Proteomics identification of differentially expressed proteins associated with pollen germination and tube growth reveals characteristics of germinated Oryza sativa pollen. *Mol. Cell. Proteomics* **2007**, *6* (2), 207−30.
(40) Boutte, Y.; Men, S.; Grebe, M. Fluorescent in situ visualization of sterols in Arabidopsis roots. *Nat. Protoc.* **2011**, *6* (4), 446−56.
(41) Bradford, M. M. A rapid and sensitive method for the quantitation of microgram quantities of protein utilizing the principle of protein-dye binding. *Anal. Biochem.* **1976**, *72*, 248−54.
(42) Han, B.; Chen, S.; Dai, S.; Yang, N.; Wang, T. Isobaric tags for relative and absolute quantification- based comparative proteomics reveals the features of plasma membrane-associated proteomes of pollen grains and pollen tubes from Lilium davidii. *J. Integr. Plant Biol.* **2010**, *52* (12), 1043−58.
(43) Morel, J.; Claverol, S.; Mongrand, S.; Furt, F.; Fromentin, J.; Bessoule, J. J.; Blein, J. P.; Simon-Plas, F. Proteomics of plant detergent-resistant membranes. *Mol. Cell. Proteomics* **2006**, *5* (8), 1396−411.
(44) Wachtler, V.; Balasubramanian, M. K. Yeast lipid rafts?−an emerging view. *Trends Cell Biol.* **2006**, *16* (1), 1−4.
(45) Grebe, M.; Xu, J.; Mobius, W.; Ueda, T.; Nakano, A.; Geuze, H. J.; Rook, M. B.; Scheres, B. Arabidopsis sterol endocytosis involves actin-mediated trafficking via ARA6-positive early endosomes. *Curr. Biol.* **2003**, *13* (16), 1378−87.

DOI: 10.1021/acs.jproteome.7b00852
J. Proteome Res. 2018, 17, 1532−1546

(46) Moscatelli, A.; Gagliardi, A.; Maneta-Peyret, L.; Bini, L.; Stroppa, N.; Onelli, E.; Landi, C.; Scali, M.; Idilli, A. I.; Moreau, P. Characterisation of detergent-insoluble membranes in pollen tubes of Nicotiana tabacum (L.). *Biol. Open* **2015**, *4* (3), 378−99.
(47) Roche, Y.; Gerbeau-Pissot, P.; Buhot, B.; Thomas, D.; Bonneau, L.; Gresti, J.; Mongrand, S.; Perrier-Cornet, J. M.; Simon-Plas, F. Depletion of phytosterols from the plant plasma membrane provides evidence for disruption of lipid rafts. *FASEB J.* **2008**, *22* (11), 3980−91.
(48) Dermine, J. F.; Duclos, S.; Garin, J.; St-Louis, F.; Rea, S.; Parton, R. G.; Desjardins, M. Flotillin-1-enriched lipid raft domains accumulate on maturing phagosomes. *J. Biol. Chem.* **2001**, *276* (21), 18507−12.
(49) Sasaki, Y.; Oshima, Y.; Koyama, R.; Maruyama, R.; Akashi, H.; Mita, H.; Toyota, M.; Shinomura, Y.; Imai, K.; Tokino, T. Identification of flotillin-2, a major protein on lipid rafts, as a novel target of p53 family members. *Mol. Cancer Res.* **2008**, *6* (3), 395−406.
(50) Haney, C. H.; Long, S. R. Plant flotillins are required for infection by nitrogen-fixing bacteria. *Proc. Natl. Acad. Sci. U. S. A.* **2010**, *107* (1), 478−83.
(51) Alexandersson, E.; Gustavsson, N.; Bernfur, K.; Kjellbom, P.; Larsson, C. Plasma Membrane Proteomics. In Šamaj, J., Thelen, J. J., Eds.; *Plant Proteomics*; Springer: Berlin, Heidelberg, 2007; pp 186−206.
(52) Peltier, J. B.; Ytterberg, A. J.; Sun, Q.; van Wijk, K. J. New functions of the thylakoid membrane proteome of Arabidopsis thaliana revealed by a simple, fast, and versatile fractionation strategy. *J. Biol. Chem.* **2004**, *279* (47), 49367−83.
(53) Tang, H. Y.; Beer, L. A.; Barnhart, K. T.; Speicher, D. W. Rapid verification of candidate serological biomarkers using gel-based, label-free multiple reaction monitoring. *J. Proteome Res.* **2011**, *10* (9), 4005−17.
(54) Yang, Z. Cell polarity signaling in Arabidopsis. *Annu. Rev. Cell Dev. Biol.* **2008**, *24*, 551−75.
(55) Feraru, E.; Feraru, M. I.; Kleine-Vehn, J.; Martinière, A.; Mouille, G.; Vanneste, S.; Vernhettes, S.; Runions, J.; Friml, J. PIN polarity maintenance by the cell wall in Arabidopsis. *Curr. Biol.* **2011**, *21* (4), 338−43.
(56) Garofalo, T.; Manganelli, V.; Grasso, M.; Mattei, V.; Ferri, A.; Misasi, R.; Sorice, M. Role of mitochondrial raft-like microdomains in the regulation of cell apoptosis. *Apoptosis* **2015**, *20* (5), 621−34.
(57) Sorice, M.; Mattei, V.; Tasciotti, V.; Manganelli, V.; Garofalo, T.; Misasi, R. Trafficking of PrPc to mitochondrial raft-like microdomains during cell apoptosis. *Prion* **2012**, *6* (4), 354−8.
(58) Lefebvre, B.; Furt, F.; Hartmann, M. A.; Michaelson, L. V.; Carde, J. P.; Sargueil-Boiron, F.; Rossignol, M.; Napier, J. A.; Cullimore, J.; Bessoule, J. J.; Mongrand, S. Characterization of lipid rafts from *Medicago truncatula* root plasma membranes: a proteomic study reveals the presence of a raft-associated redox system. *Plant Physiol.* **2007**, *144* (1), 402−18.
(59) Navarre, C.; Degand, H.; Bennett, K. L.; Crawford, J. S.; Mortz, E.; Boutry, M. Subproteomics: identification of plasma membrane proteins from the yeast. *Proteomics* **2002**, *2* (12), 1706−14.
(60) Alexandersson, E.; Saalbach, G.; Larsson, C.; Kjellbom, P. *Arabidopsis* plasma membrane proteomics identifies components of transport, signal transduction and membrane trafficking. *Plant Cell Physiol.* **2004**, *45* (11), 1543−56.
(61) Xiao, W.; Zhou, S.; Xu, H.; Li, H.; He, G.; Liu, Y.; Qi, Y. Nogo-B promotes the epithelial-mesenchymal transition in HeLa cervical cancer cells via Fibulin-5. *Oncol. Rep.* **2013**, *29* (1), 109−16.
(62) Brugger, B.; Sandhoff, R.; Wegehingel, S.; Gorgas, K.; Malsam, J.; Helms, J. B.; Lehmann, W. D.; Nickel, W.; Wieland, F. T. Evidence for segregation of sphingomyelin and cholesterol during formation of COPI-coated vesicles. *J. Cell Biol.* **2000**, *151* (3), 507−18.
(63) Greaves, J.; Chamberlain, L. H. Palmitoylation-dependent protein sorting. *J. Cell Biol.* **2007**, *176* (3), 249−54.
(64) Raffaele, S.; Bayer, E.; Lafarge, D.; Cluzet, S.; German Retana, S.; Boubekeur, T.; Leborgne-Castel, N.; Carde, J. P.; Lherminier, J.; Noirot, E.; Satiat-Jeunemaître, B.; Laroche-Traineau, J.; Moreau, P.; Ott, T.; Maule, A. J.; Reymond, P.; Simon-Plas, F.; Farmer, E. E.; Bessoule, J. J.; Mongrand, S. Remorin, a solanaceae protein resident in membrane rafts and plasmodesmata, impairs potato virus X movement. *Plant Cell* **2009**, *21* (5), 1541−55.
(65) Furt, F.; Konig, S.; Bessoule, J. J.; Sargueil, F.; Zallot, R.; Stanislas, T.; Noirot, E.; Lherminier, J.; Simon-Plas, F.; Heilmann, I.; Mongrand, S. Polyphosphoinositides are enriched in plant membrane rafts and form microdomains in the plasma membrane. *Plant Physiol.* **2010**, *152* (4), 2173−87.
(66) Ressayre, A.; Mignot, A.; Siljak-Yakovlev, S.; Raquin, C. Postmeiotic cytokinesis and pollen aperture number determination in eudicots: effect of the cleavage wall number. *Protoplasma.* **2003**, *221* (3−4), 257−68.
(67) Grison, M. S.; Brocard, L.; Fouillen, L.; Nicolas, W.; Wewer, V.; Dörmann, P.; Nacir, H.; Benitez-Alfonso, Y.; Claverol, S.; Germain, V.; Boutté, Y.; Mongrand, S.; Bayer, E. M. Specific membrane lipid composition is important for plasmodesmata function in Arabidopsis. *Plant Cell* **2015**, *27* (4), 1228−50.
(68) Gu, Y.; Fu, Y.; Dowd, P.; Li, S.; Vernoud, V.; Gilroy, S.; Yang, Z. A Rho family GTPase controls actin dynamics and tip growth via two counteracting downstream pathways in pollen tubes. *J. Cell Biol.* **2005**, *169* (1), 127−38.
(69) Zhao, Y.; Yan, A.; Feijó, J. A.; Furutani, M.; Takenawa, T.; Hwang, I.; Fu, Y.; Yang, Z. Phosphoinositides regulate clathrin-dependent endocytosis at the tip of pollen tubes in Arabidopsis and tobacco. *Plant Cell* **2010**, *22* (12), 4031−44.
(70) Heilmann, I.; Ischebeck, T. Male functions and malfunctions: the impact of phosphoinositides on pollen development and pollen tube growth. *Plant Reprod.* **2016**, *29* (1−2), 3−20.
(71) Zárský, V.; Cvrcková, F.; Potocký, M.; Hála, M. Exocytosis and cell polarity in plants - exocyst and recycling domains. *New Phytol.* **2009**, *183* (2), 255−72.
(72) He, B.; Xi, F.; Zhang, X.; Zhang, J.; Guo, W. Exo70 interacts with phospholipids and mediates the targeting of the exocyst to the plasma membrane. *EMBO J.* **2007**, *26* (18), 4053−65.
(73) Liu, J.; Zuo, X.; Yue, P.; Guo, W. Phosphatidylinositol 4,5-bisphosphate mediates the targeting of the exocyst to the plasma membrane for exocytosis in mammalian cells. *Mol. Biol. Cell* **2007**, *18* (11), 4483−92.
(74) Hála, M.; Cole, R.; Synek, L.; Drdová, E.; Pecenková, T.; Nordheim, A.; Lamkemeyer, T.; Madlung, J.; Hochholdinger, F.; Fowler, J. E.; Zárský, V. An exocyst complex functions in plant cell growth in Arabidopsis and tobacco. *Plant Cell* **2008**, *20* (5), 1330−45.
(75) Shen, J.; Tareste, D. C.; Paumet, F.; Rothman, J. E.; Melia, T. J. Selective activation of cognate SNAREpins by Sec1/Munc18 proteins. *Cell* **2007**, *128* (1), 183−95.
(76) Essid, M.; Gopaldass, N.; Yoshida, K.; Merrifield, C.; Soldati, T. Rab8a regulates the exocyst-mediated kiss-and-run discharge of the Dictyostelium contractile vacuole. *Mol. Biol. Cell* **2012**, *23* (7), 1267−82.
(77) Vidal-Quadras, M.; Holst, M. R.; Francis, M. K.; Larsson, E.; Hachimi, M.; Yau, W. L.; Peränen, J.; Martín-Belmonte, F.; Lundmark, R. Endocytic turnover of Rab8 controls cell polarization. *J. Cell Sci.* **2017**, *130* (6), 1147−1157.
(78) Bosch, M.; Hepler, P. K. Pectin methylesterases and pectin dynamics in pollen tubes. *Plant Cell* **2005**, *17* (12), 3219−26.
(79) Jiang, J.; Yao, L.; Yu, Y.; Lv, M.; Miao, Y.; Cao, J. PECTATE LYASE-LIKE10 is associated with pollen wall development in Brassica campestris. *J. Integr. Plant Biol.* **2014**, *56* (11), 1095−105.
(80) Lyu, M.; Yu, Y.; Jiang, J.; Song, L.; Liang, Y.; Ma, Z.; Xiong, X.; Cao, J. BcMF26a and BcMF26b Are Duplicated Polygalacturonase Genes with Divergent Expression Patterns and Functions in Pollen Development and Pollen Tube Formation in Brassica campestris. *PLoS One* **2015**, *10* (7), e0131173.
(81) Mollet, J. C.; Leroux, C.; Dardelle, F.; Lehner, A. Cell Wall Composition, Biosynthesis and Remodeling during Pollen Tube Growth. *Plants* **2013**, *2* (1), 107−47.
(82) Cosgrove, D. J. Catalysts of plant cell wall loosening. [version 1; referees: 2 approved]. *F1000Research* **2016**, *5* (F1000 Faculty Rev.), 119.
(83) Ulstrup, J. C.; Jeansson, S.; Wiker, H. G.; Harboe, M. Relationship of secretion pattern and MPB70 homology with osteoblast-specific

DOI: 10.1021/acs.jproteome.7b00852
J. Proteome Res. 2018, 17, 1532−1546

factor 2 to osteitis following Mycobacterium bovis BCG vaccination. *Infect. Immun.* **1995**, *63* (2), 672−5.
(84) Huber, O.; Sumper, M. Algal-CAMs: isoforms of a cell adhesion molecule in embryos of the alga Volvox with homology to Drosophila fasciclin I. *EMBO J.* **1994**, *13* (18), 4212−22.
(85) Araújo, S. J.; Tear, G. Axon guidance mechanisms and molecules: lessons from invertebrates. *Nat. Rev. Neurosci.* **2003**, *4* (11), 910−22.
(86) Huang, G. Q.; Gong, S. Y.; Xu, W. L.; Li, W.; Li, P.; Zhang, C. J.; Li, D. D.; Zheng, Y.; Li, F. G.; Li, X. B. A fasciclin-like arabinogalactan protein, GhFLA1, is involved in fiber initiation and elongation of cotton. *Plant Physiol.* **2013**, *161* (3), 1278−90.

DOI: 10.1021/acs.jproteome.7b00852
J. Proteome Res. 2018, 17, 1532−1546